

UC San Diego

UC San Diego Previously Published Works

Title

Untangling irrigation effects on maize water and heat stress alleviation using satellite data

Permalink

<https://escholarship.org/uc/item/0j4491kt>

Journal

Hydrology and Earth System Sciences, 26(3)

ISSN

1027-5606

Authors

Zhu, Peng
Burney, Jennifer

Publication Date

2022

DOI

10.5194/hess-26-827-2022

Peer reviewed



1 **Untangling irrigation effects on maize water and heat stress**
2 **alleviation using satellite data**

3
4 Peng Zhu^{1*}, Jennifer Burney¹

5 ¹School of Global Policy and Strategy, University of California, San Diego, CA USA

6 *Correspondence to:* Peng Zhu (zhuyp678@gmail.com)

7
8 **Abstract.** Irrigation has important implications for sustaining global food production,
9 enabling crop water demand to be met even under dry conditions. Added water also
10 cools crop plants through transpiration; irrigation might thus play an important role in
11 a warmer climate by simultaneously moderating water and high temperature stresses.
12 Here we use satellite-derived evapotranspiration estimates, land surface temperature
13 (LST) measurements, and crop phenological stage information from Nebraska maize
14 to quantify how irrigation relieves both water and temperature stresses. Our study
15 shows that, unlike air temperature metrics, satellite-derived LST detects significant
16 irrigation-induced cooling effect, especially during the grain filling period (GFP) of
17 crop growth. This cooling is likely to extend the maize growing season, especially for
18 GFP, likely due to the stronger temperature sensitivity of phenological development
19 during this stage. The analysis also suggests that irrigation not only reduces water and
20 temperature stress but also weakens the response of yield to these stresses.
21 Specifically, temperature stress is significantly weakened for reproductive processes
22 in irrigated crops. The attribution analysis further suggests that water and high
23 temperature stress alleviation contributes to 65% and 35% of yield benefit,
24 respectively. Our study underlines the relative importance of high temperature stress
25 alleviation in yield improvement and the necessity of simulating crop surface
26 temperature to better quantify heat stress effects in crop yield models. Finally,
27 untangling irrigation effects on both heat and water stress mitigation has important
28 implications for designing agricultural adaptation strategies under climate change.

29

30 **Keywords:** Irrigation, Evaporative cooling, MODIS LST, High temperature
31 stress, Water stress, Maize

32



33 1. Introduction

34 Irrigation -- a large component of freshwater consumption sourced from water
35 diversion from streams and groundwater (Wallace, 2000, Howell, 2001) -- allows
36 crops to grow in environments that do not receive sufficient rainfall, and buffers
37 agricultural production from climate variability and extremes. Irrigated agriculture
38 plays an outsized role in global crop production and food security: irrigated lands
39 account for 17% of total cropped area, yet they provide 40% of global cereals
40 (Rosegrant et al 2002, Siebert and Döl 2010). Meeting the rising food demands of a
41 growing global population will require either increasing crop productivity and/or
42 expansion of cropped areas; both strategies are daunting under projected climate
43 change. Cropland expansion may be in marginal areas that require irrigation even in
44 the present climate (Bruinsma 2009); increasing temperatures will drive higher
45 atmospheric vapor pressure deficits (VPD) and raise crop water demand and crop
46 water losses. This increasing water demand poses a water ceiling for crop growth and
47 might necessitate irrigation application over present rainfed areas to increase or even
48 maintain yields (DeLucia et al., 2019).

49

50 However, the provision of additional irrigation water modifies both the land surface
51 water and energy budgets. Additional water can result in an evaporative cooling
52 effect, which may be beneficial for crop growth indirectly through lowering the
53 frequency of extreme heat stress (Butler et al., 2018). Especially considering the
54 future warmer climate, high temperature stress will be more prevalent (Russo et al.,
55 2014) and might result in more severe yield losses than water stress (Zhu et al., 2019)
56 due to reduced photosynthesis, pollen sterility, and accelerated crop senescence in
57 major cereals (Rezaei et al., 2015b; Rattalino Edreira et al., 2011; Ruiz-Vera et al.,
58 2018), therefore, a better understanding of irrigation effect on high temperature stress
59 alleviation will be important for agricultural management practices. More broadly,
60 understanding how irrigation can or should contribute to a portfolio of agricultural
61 adaptation strategies thus requires improved understanding of its relative roles in
62 mitigating both water and heat stresses.

63

64 Climate models and meteorological data have been used to investigate how historical
65 expansion of irrigation at global and regional scales has influenced the climate



66 system, including surface cooling and precipitation variation (Kang and Eltahir, 2019;
67 Thiery et al., 2017; Bonfils and Lobell, 2007; Sacks et al., 2009). However, many
68 crop models still use air temperature rather than canopy temperature to estimate heat
69 stress; this may overestimate heat stress effect in irrigated cropland (Siebert et al.,
70 2017), since canopy temperature can deviate significantly from air temperature
71 depending on the crop moisture conditions (Siebert et al., 2014). Recently, a
72 comparison of crop model simulated canopy temperature suggests that most crop
73 models lack a sufficient ability to reproduce the field-measured canopy temperature,
74 even for models with a good performance in grain yield simulation (Webber et al.,
75 2017).

76

77 Alternatively, satellite-derived land surface temperature (LST) has been used to
78 directly quantify regional scale surface warming or cooling effects resulting from
79 surface energy budget changes due to changes in land cover and land management
80 (Loarie et al., 2011; Tomlinson et al., 2012; Peng et al., 2014). Importantly, yield
81 prediction model comparisons suggest that replacing air temperature with MODIS
82 LST can improve yield predictions because LST accounts for both evaporative
83 cooling and water stress (Li et al., 2019). Satellite data also provide the observational
84 evidence to constrain model performance or directly retrieve crop growth status
85 information. For example, satellite derived soil moisture had been used to characterize
86 irrigation pattern and improve irrigation amount estimation (Felfelani et al., 2018;
87 Lawston et al., 2017; Jalilvand et al., 2019; Zaussinger et al., 2019). Therefore,
88 integrating satellite products have the potential to improve our understanding of how
89 irrigation and climate change impact crop yield and thus provide guides for farmers to
90 make the optimal decisions.

91

92 In this study, we focus on Nebraska, the third largest maize producer in the United
93 States. Multi-year mean climate data shows that conditions are drier in western areas
94 and warmer in southern areas (Figure 1a and b). Importantly, Nebraska features a
95 mixture of irrigated and rainfed maize that facilitates comparison (more than half
96 (56%) of the Nebraska maize cropland is irrigated with more irrigated maize in the
97 western area (Figure 1c), according to the United States Department of Agriculture
98 (USDA, 2018a)). County yield data from the USDA shows that interannual
99 fluctuations in rainfed maize yield are much larger than for irrigated maize (Figure



100 1b). Although irrigated yields are higher, rainfed maize yields have grown faster than
101 irrigated (3.9% per year versus 1.0% per year) over the study period (2003-2016)
102 (Figure 1b), one of the possible reasons is that breeding technology progress has
103 improved the drought tolerance of maize hybrids (Messina et al., 2010).

104

105 As noted above, irrigation potentially benefits crop yields by moderating both water
106 and high temperature stress. Here we use satellite-derived LST and satellite-derived
107 water stress metrics to statistically tease apart the contributions of irrigation to water
108 and heat stress alleviation, separately. We: (1) evaluate the difference in temperature
109 and moisture conditions over irrigated and rainfed maize croplands; (2) explore how
110 irrigation mitigates water and high temperature stresses using panel statistical models;
111 (3) quantify the relative contributions of irrigation-induced water and high
112 temperature stress alleviation to yield improvements; and (4) explore whether current
113 crop models can reproduce the observed irrigation benefits on maize growth status.

114 **2. Materials and Methods**

115 We first describe the data used, followed by a brief description of statistical
116 methodology.

117 **2.1 Satellite products to identify irrigated and non-irrigated maize areas**

118 We used the United States Department of Agriculture's Cropland Data Layer (CDL)
119 to identify maize croplands for each year in the study period 2003-2016 (USDA,
120 2018b). The irrigation distribution map across Nebraska was obtained from a previous
121 study that used Landsat-derived plant greenness and moisture information to create a
122 continuous annual irrigation map across U.S. Northern High Plains (Deines et al.,
123 2017). The irrigation map showed a very high accuracy (92 to 100%) when validated
124 with randomly generated test points and also highly correlated with county statistics
125 ($R^2 = 0.88-0.96$) (Deines et al., 2017). Both the CDL and irrigation map are at 30m
126 resolution. We first projected them to MODIS sinusoidal projection and then
127 aggregated them to 1km resolution to align with MODIS ET and LST products. Then,
128 pixels containing more than 60% maize and an irrigation fraction >60% were labeled
129 as irrigated maize while pixels with >60% maize and <10% irrigation fraction were
130 labeled as rainfed maize croplands. As always, threshold selection involves a tradeoff
131 between mixing samples and retaining as many samples as possible. Our choices of



132 <10% as the threshold for rainfed maize and 60% to define irrigated maize
133 represented the best optimization in our sample, as we found that more stringent
134 threshold had a very small effect on LST differences between irrigated and rainfed
135 maize at county level but resulted in significant data omission (more details in
136 supplementary Figure 1-2).

137

138 2.2 Maize phenology information

139 Maize growth stage information derived in a previous study was used to assess the
140 influence of irrigation on maize growth during different growth stages (Zhu et al.,
141 2018). Stage information including emergence date, silking date, and maturity date,
142 was derived with MODIS WDRVI (Wide Dynamic Range Vegetation Index, 8-day
143 and 250m resolution) based on a hybrid method combining shape model fitting (SMF)
144 and threshold-based analysis. Then we defined vegetative period (VP) as period from
145 emergence date to silking date, grain filling period (GFP) as period from silking date
146 to maturity date and growing season (GS) as period from emergence date to maturity
147 date. Details can be found in our previous studies (Zhu et al., 2018). WDRVI was
148 used due to its higher sensitivity to changes at high biomass than other vegetation
149 indices (Gitelson et al., 2004) and was estimated with the following equation:

$$150 \quad NDVI = (\rho_{NIR} - \rho_{red}) / (\rho_{NIR} + \rho_{red}) \quad (1)$$

$$151 \quad WDRVI = 100 * \frac{[(\alpha - 1) + (\alpha + 1) \times NDVI]}{[(\alpha + 1) + (\alpha - 1) \times NDVI]} \quad (2)$$

152 where ρ_{red} and ρ_{NIR} were the MODIS surface reflectance in the red and NIR bands,
153 respectively. To minimize the effects of aerosols, we used the 8-day composite
154 products in MOD09Q1 and MYD09Q1 and quality-filtered the reflectance data using
155 the band quality control flags. Only data passing the highest quality control were
156 retained (Zhu et al., 2018). The scaling factor, $\alpha=0.1$, was adopted based on a
157 previous study to degrade the fraction of the NIR reflectance at moderate-to-high
158 green vegetation and best linearly capture the maize green leaf area index (LAI)
159 (Guindin-Garcia *et al.*, 2012).

160 2.3 Temperature exposure during maize growth

161 We used daily 1-km spatial resolution MODIS Aqua LST (MYD11A1) data to
162 characterize the crop surface temperature; since its overpassing time is at 1:30 and
163 13:30, it is closer to the times of daily minimum and maximum temperature than the



164 MODIS Terra LST (Wan et al., 2008) and is therefore better for characterizing crop
165 surface temperature stress (Johnson 2016; Li et al., 2019). For quality control, pixels
166 with an LST error >3 degree were filtered out based on the corresponding MODIS
167 LST quality assurance layers. Missing values (less than 3%) were interpolated with
168 robust spline function (Teuling et al., 2010). Aqua LST data are available after July
169 2002; we thus restricted our study to the period 2003-2016. For comparison, we also
170 obtained minimum and maximum daily surface air temperature (Tmin and Tmax) at
171 1-km resolution from Daymet version 3 (Thornton et al., 2018). For both MODIS
172 LST and air temperature, we calculated integrated crop heat exposure -- the growing
173 degree days (GDD) and extreme degree days (EDD) -- with the following equations:

$$174 \quad GDD_8^{30} = \sum_{t=1}^N DD_t, \quad DD_t = \begin{cases} 0, & \text{when } T < 8^\circ\text{C} \\ T - 8, & \text{when } 8^\circ\text{C} \leq T < 30^\circ\text{C} \\ 22, & \text{when } T \geq 30^\circ\text{C} \end{cases} \quad (3)$$

$$175 \quad EDD_{30}^{\infty} = \sum_{t=1}^N DD_t, \quad DD_t = \begin{cases} 0, & \text{when } T < 30^\circ\text{C} \\ T - 30, & \text{when } T \geq 30^\circ\text{C} \end{cases} \quad (4)$$

176 Here temperature (T) could be either air temperature or LST and had been
177 interpolated from daily to hourly values with sine function (Tack *et al.*, 2017). t
178 represents the hourly time step, N is the total number of hours in a specified growing
179 period (either the entire growing season, or a specific phenological growth phase, as
180 defined below).

181

182 2.4 Maize Water Stress

183 Water stress during maize growth was characterized by the ratio of evapotranspiration
184 (ET) to potential evapotranspiration (PET), as used in previous study (Mu et al., 2013).
185 MODIS product (MYD16A2) provided both ET and PET from 2003 to 2016 and
186 showed good performance for natural vegetation (Mu et al., 2011), however, our
187 comparison using flux tower observed ET at an irrigated maize site at Nebraska
188 suggested that ET at the irrigated maize was significantly underestimated by MODIS
189 ET (Supplementary Figure 3). Therefore, we used another ET product (SSEBop ET)
190 to replace MODIS ET. SSEBop ET was also estimated with MODIS products (Senay
191 et al., 2013), like LST, vegetation index, and albedo as input variables, but used a
192 revised algorithm including predefined boundary conditions for hot and cold reference
193 pixels (Senay et al., 2013) and showed better performance than MODIS ET (Velpuri



194 et al., 2013), which was confirmed when we compared it with flux tower observed ET
195 at an irrigated maize site (Supplementary Figure 4). The comparison of MODIS PET
196 and flux tower estimated PET shows MODIS PET has satisfactory performance
197 (Supplementary Figure 5). Since MODIS PET from MYD16A2 has a spatial
198 resolution of 500 m with 8-day temporal resolution, while SSEBop ET has 1km
199 spatial resolution with daily time step, we reconciled the two datasets to 1km spatial
200 resolution and 8-day temporal resolution. Then ET, PET and ET/PET were averaged
201 over time to get mean ET, PET and ET/PET during VP, GFP and GS with satellite
202 derived phenology to characterize water status during maize growth.

203 **2.5 Crop model simulation results**

204 We compared the results of our statistical analysis with four gridded crop models.
205 Simulation results from pAPSIM, pDSSAT, LPJ-GUESS, CLM-crop for both rainfed
206 and irrigated maize across Nebraska were obtained from Agricultural Model
207 Intercomparison and Improvement Project (AgMIP) (Rosenzweig *et al.*, 2013) and
208 Inter-Sectoral Impact Model Intercomparison Project 1 (ISIMIP1) (Warszawski *et al.*,
209 2014). The four models were driven by the same climate forcing dataset (AgMERRA)
210 and run at a spatial resolution of 0.5 arc-degree longitude and latitude. All simulations
211 were conducted for purely rainfed and near-perfectly irrigated conditions. These
212 models simulated maize yield, total biomass, ET and growing stage information
213 (planting date, flowering date and maturity date). Planting date occurs on the first day
214 following the prescribed sowing date in which soil temperature is at least 2 degrees
215 above the 8 °C base temperature. Harvest occurs once the specified heat units are
216 reached. Heat units to maturity were calibrated from the prescribed crop calendar data
217 (Elliott *et al.*, 2015). Crop model simulation was evaluated by calculating the Pearson
218 correlation between simulated yields in the baseline simulations and detrended
219 historical yields for each country from the Food and Agriculture Organization.
220 Management scenario ‘harmon’ was selected, meaning the simulation using
221 harmonized fertilizer inputs and assumptions on growing seasons. More details on the
222 simulation protocol can be found in Elliott *et al.* (2015) and Mueller *et al.* (2019). We
223 used this model comparison project outputs to shed light on how well crop models
224 had simulated the irrigation benefits we identified in different phases of crop growth.



225 **2.6 Method**

226 We used standard panel statistical analysis techniques to identify the impacts of
227 irrigation on maize productivity via heat stress reduction and water stress reduction
228 pathways.

229

230 Comparison of LST, ET, PET, ET/PET, GDD and EDD between irrigated and rainfed
231 maize areas was performed within each county to minimize the effects of other
232 spatially-varying factors, like background temperature and management practices, on
233 surface temperature and evapotranspiration. These biophysical variables averaged
234 over each county were then integrated over vegetative period (VP, from emergence
235 date to silking date), grain filling period (GFP, from silking date to maturity date) and
236 whole growing season (GS, from emergence date to maturity date) so we could
237 evaluate whether and how irrigation had differentially influenced maize growth
238 during early VP and late GFP.

239

240 We further examined how irrigation had changed the sensitivity of maize yield and its
241 components to temperature variation. As done in our previous study (Zhu et al., 2019),
242 we decomposed the total yield variation into three components: biomass growth rate
243 (BGR), growing season length (GSL) and harvest index (HI) based on the following
244 equation:

$$245 \text{Yield} = HI \cdot AGB = HI \cdot BGR \cdot GSL \quad (5)$$

246 Aboveground biomass (AGB) was retrieved through a regression model:

$$247 \text{AGB} = 16.4 \cdot \text{IWDRVI}^{0.8} \quad (6)$$

248 which was built in the previous study through regressing field measured maize AGB
249 against MODIS derived integrated WDRVI (IWDRVI) (Zhu et al., 2019). Then HI
250 could be estimated as Yield/AGB and BGR could be estimated as AGB/GSL . Such
251 decomposition allowed us to examine how different crop growth physiological
252 processes responded to external forcing: HI characterizes dry matter partitioning
253 between source organ and sink organ and is mainly related with processes
254 determining grain size and grain weight; BGR is related with physiological processes
255 of daily carbon assimilation rate through photosynthesis and GSL is related with crop
256 phenological development. The uncertainties related with AGB estimation was
257 quantified through resampling as we did in previous studies (Zhu et al., 2019).

258



259 Temperature sensitivity of irrigated or rainfed yield (S_T^{Yield}) was estimated using a
 260 panel data model (Eq. (7)) with growing season mean LST and ET/PET as the
 261 explanatory variables:

$$262 \quad \log(Yield_{i,t}) = \gamma_1 t + \gamma_2 LST_{i,t} + \gamma_3 \frac{ET}{PET}_{i,t} + County_i + \varepsilon_{i,t} \quad (7)$$

263 $Yield_{i,t}$ is maize yield (t/ha) in county i and year t . It was a function of overall yield
 264 trends ($\gamma_1 t$) that had fairly steadily increased over the study period (Figure 1b), local
 265 crop temperature stress ($LST_{i,t}$), and local crop water stress ($\frac{ET}{PET}_{i,t}$). The $County_i$
 266 terms provided an independent intercept for each county (fixed effect), and thus
 267 accounted for time-invariant county-level differences that contributed to variations in

268 yield, like the soil quality. $\varepsilon_{i,t}$ is an idiosyncratic error term. γ_2 or $\frac{\partial \ln(Yield)}{\partial LST}$ defines
 269 the temperature sensitivity of yield. The temperature sensitivity of BGR (S_T^{BGR}), HI
 270 (S_T^{HI}) and GSL (S_T^{GSL}) could be estimated with Eq (7) in a similar way through using
 271 BGR, HI and GSL as the dependent variable. Here the dependent variable Yield
 272 (BGR, GSL and HI) was logged, so the estimated temperature sensitivity represented
 273 the percentage change of Yield (BGR, GSL and HI) with 1 °C temperature increase.

274

275 To quantify the relative contribution of water and high temperature stress alleviation
 276 to yield benefit, the yield difference between irrigated and non-irrigated maize
 277 (irrigation yield-rainfed yield, $\Delta Yield$) was regressed over the quadratic function of
 278 growing season EDD and ET/PET differences between irrigated and rainfed maize:

$$279 \quad \Delta Yield_{i,t} = \gamma_1 \Delta \frac{ET}{PET}_{i,t} + \gamma_2 \Delta \frac{ET}{PET}_{i,t}^2 + \gamma_3 \Delta EDD_{i,t} + \gamma_4 \Delta EDD_{i,t}^2 + County_i + \varepsilon_{i,t} \quad (8)$$

280 The yield improvement explained by heat and water stress alleviation was estimated

$$281 \quad \text{as } \frac{\gamma_1 \sum \Delta \frac{ET}{PET}_{i,t} + \gamma_2 \sum \Delta \frac{ET}{PET}_{i,t}^2 + \gamma_3 \sum \Delta EDD_{i,t} + \gamma_4 \sum \Delta EDD_{i,t}^2}{\sum \Delta Yield_{i,t}} \quad . \quad \text{The relative}$$

282 contribution of water and high temperature stress alleviation was estimated as

$$283 \quad \frac{\gamma_1 \sum \Delta \frac{ET}{PET}_{i,t} + \gamma_2 \sum \Delta \frac{ET}{PET}_{i,t}^2}{\gamma_1 \sum \Delta \frac{ET}{PET}_{i,t} + \gamma_2 \sum \Delta \frac{ET}{PET}_{i,t}^2 + \gamma_3 \sum \Delta EDD_{i,t} + \gamma_4 \sum \Delta EDD_{i,t}^2} \quad \text{and}$$



284
$$\frac{\gamma_3 \sum \Delta EDD_{i,t} + \gamma_4 \sum \Delta EDD_{i,t}^2}{\gamma_1 \sum \Delta \frac{ET}{PET}_{i,t} + \gamma_2 \sum \Delta \frac{ET}{PET}_{i,t}^2 + \gamma_3 \sum \Delta EDD_{i,t} + \gamma_4 \sum \Delta EDD_{i,t}^2}$$
, respectively. Given
 285 the potential collinearity between $\Delta \frac{ET}{PET}$ and ΔEDD , we also calculated the Variance
 286 inflation factor (VIF) to diagnose the severity of collinearity. The daytime LST
 287 difference (ΔLST) was also tested to characterize heat stress alleviation with the
 288 following equation:

289
$$\Delta Yield_{i,t} = \gamma_1 \Delta \frac{ET}{PET}_{i,t} + \gamma_2 \Delta \frac{ET}{PET}_{i,t}^2 + \gamma_3 \Delta LST_{i,t} + \gamma_4 \Delta LST_{i,t}^2 + County_i + \varepsilon_{i,t} \quad (9)$$

290 Then, the relative contribution of water and high temperature stress alleviation was

291 estimated as
$$\frac{\gamma_1 \sum \Delta \frac{ET}{PET}_{i,t} + \gamma_2 \sum \Delta \frac{ET}{PET}_{i,t}^2}{\gamma_1 \sum \Delta \frac{ET}{PET}_{i,t} + \gamma_2 \sum \Delta \frac{ET}{PET}_{i,t}^2 + \gamma_3 \sum \Delta LST_{i,t} + \gamma_4 \sum \Delta LST_{i,t}^2}$$
 and
 292
$$\frac{\gamma_3 \sum \Delta LST_{i,t} + \gamma_4 \sum \Delta LST_{i,t}^2}{\gamma_1 \sum \Delta \frac{ET}{PET}_{i,t} + \gamma_2 \sum \Delta \frac{ET}{PET}_{i,t}^2 + \gamma_3 \sum \Delta LST_{i,t} + \gamma_4 \sum \Delta LST_{i,t}^2}$$
, respectively.

293 3. Results

294 As expected, irrigation improved maize yield and the yield benefit showed a distinct
 295 spatial variation when we compared areas we identified as irrigated versus rainfed
 296 maize. The yield benefit of irrigation was much higher in the western area of the state
 297 (Figure 2a), because the drier environment in western area widened the yield gap
 298 between irrigated and rainfed cropland in an average year. The satellite derived
 299 vegetation index WDRVI reflected these differences, with higher values in areas we
 300 identified as irrigated maize, especially around maize silking (Figure 2b). Importantly,
 301 this suggested that, in conjunction with ground-based information calibrated crop
 302 phenology, irrigated and rainfed cropland were distinguishable with time series
 303 satellite data where rainfall does not meet crop water demand.

304

305 When county-level LST data were averaged over 2003-2016, the daytime LST in
 306 irrigated maize was 1.5°C cooler than rainfed maize, while nighttime LST showed a
 307 very slight difference (0.2 °C) (Figure 3a,b). When the LST differences were



308 integrated over different growing periods (Figure 3e-h), we found that the daytime
309 cooling effect was greatest in the GFP (Figure 3g), probably due to the higher LAI (or
310 ground cover) and transpiration during that stage of growth. This was also consistent
311 with previous field studies showing that irrigation was mainly applied during the
312 middle to late reproductive period, which corresponded to the greatest water demand
313 period (Chen et al., 2018). The spatial pattern of the LST difference showed stronger
314 cooling effect in the western area (Figure 3c-h), which was similar to the spatial
315 pattern of yield benefit identified in Figure 2a. In contrast, surface air temperature
316 shows much smaller daytime cooling effect (Figure 3i,j). The mean air temperature
317 difference between irrigated and rainfed maize in daytime and nighttime were -0.2°C
318 and -0.3°C , respectively, and the spatial pattern of air temperature difference over VP
319 and GFP was also relatively small between counties and crop growth periods (Figure
320 3k-p).

321

322 Temperature is an important driver of crop phenology and has been used as the
323 primary environmental variables in crop phenology models (Wang et al., 1998).
324 Given the identified irrigation cooling, we further looked into how irrigation altered
325 maize phenological stages. We found irrigated maize showed an earlier emergence
326 and silking but delayed maturity (Figure 4a). Consequently, GFP was extended by 7.5
327 days on average, which contributed to most of GS extension (8.1 days) (Figure 4b).
328 Site measurements of phenological stage information confirmed that irrigated maize
329 had a longer GS, especially during GFP (Figure 4c). The reason why such extension
330 mainly occurred in GFP might be that (1) LST cooling was more prominent during
331 GFP and (2) phenological development during GFP was more sensitive to
332 temperature variation than development during VP (Egli et al., 2004). The higher
333 temperature sensitivity of phenological development during GFP ($4.9 \text{ day}/^{\circ}\text{C}$) was
334 confirmed when we regress GFP difference between irrigated and rainfed maize over
335 LST difference between irrigated and rainfed maize (Figure 4d-f). The spatial pattern
336 suggested GS and GFP extension was more significant in the western area (Figure 4g-
337 h), likely due to the corresponding stronger cooling effect.

338

339 We integrated LST or air temperature as described above (Materials and Methods) to
340 estimate heat exposure (GDD and EDD) over maize growing season. We found both
341 LST and air temperature estimated GDD were greater in irrigated maize than GDD in



342 rainfed maize across most counties, especially during GFP (Figure 5a,c), which was
343 very likely due to the GFP extension. As GDD characterizes the beneficial thermal
344 time accumulation, the greater GDD in irrigated maize might contribute to the higher
345 yield. In terms of EDD, LST estimated EDD suggested that irrigation suppressed high
346 temperature stress especially for GFP (Figure 5b), while air temperature estimated
347 EDD failed to characterize the irrigation induced lower high temperature stress
348 (Figure 5d).

349
350 SSEBop ET and MODIS PET were used to explore how irrigation influenced water
351 demand and water supply across maize. We found irrigation led to 27% higher ET
352 and 2% lower PET (Figure 6a-b). Higher ET was anticipated in irrigated maize, and
353 lower PET might be due to irrigation cooling effect, which resulted in lower VPD and
354 thus lower evaporative demand. We used the ratio of ET to PET as the metric for
355 water stress in this study, where low values indicated that plants were not transpiring
356 at their full potential in the ambient conditions. This ratio was higher for irrigated
357 maize, especially during the GFP (Figure 6c), and the spatial distribution suggested
358 that the difference was greater in western counties than eastern counties (Figure 6d-e),
359 which was similar to the distribution of the local cooling effect identified in Figure 3c.
360

361 We divided the temperature sensitivity of yield into three components (sensitivity of
362 BGR, GSL and HI) to investigate how irrigation changed the response of maize
363 physiological processes to temperature. As shown in Figure 7, we found that
364 temperature sensitivity of yield was significantly weakened from $-6.9\%/^{\circ}\text{C}$ to
365 $-1\%/^{\circ}\text{C}$ in irrigated vs. rainfed areas, and this yield sensitivity change was mainly
366 driven by a change in the sensitivity of the HI, which was weakened from $-4.2\%/^{\circ}\text{C}$
367 to $1\%/^{\circ}\text{C}$. In both rainfed and irrigated maize, temperature sensitivity of GSL was
368 quite close (approximately $-2\%/^{\circ}\text{C}$), while BGR was only slightly influenced by
369 temperature (Figure 7).

370
371 We found that irrigation application not only lowered water and high temperature
372 stress, but also made yield less sensitive to water and high temperature stress (Figure
373 8a-c), consistent with previous studies (Troy et al., 2015; Tack et al., 2017). We
374 regressed yield differences over climatic variables differences using the linear model



375 (Eq. (8)), and estimated that 61% of yield improvement between irrigated and rainfed
376 maize could be explained by the irrigation induced heat and water stress alleviation.
377 We further calculated that 79% of yield improvement was due to water stress
378 alleviation and 21% due to heat stress alleviation. Because the distribution of ΔEDD
379 was truncated for points with $\Delta EDD > 0$ (Figure 8e), we explored an alternative model
380 with quadratic functions of ΔLST and $\Delta ET/PET$ (Eq. (9)). In this specification, 72%
381 of yield improvement can be explained by water and high temperature stress
382 alleviation, with 65% and 35% of yield improvement due to water and high
383 temperature stress alleviation, respectively. The VIF we used to diagnose the
384 collinearity between ΔLST and $\Delta ET/PET$ was 2.2. Normally, VIFs over 10 indicate
385 collinear variables (with 5 being a more strict standard), therefore, our VIF test
386 suggested the collinearity was not severe, probably because we used differences of
387 LST and ET/PET between irrigated and rainfed maize rather than directly using LST
388 and ET/PET as the explanatory variables.

389
390 Because we found a strong effect on yields via the heat stress (and not simply water
391 stress), we compared our results with four process-based crop models that simulated
392 crop growth under both rainfed and irrigated conditions. These simulations
393 qualitatively reproduced the irrigation-induced higher maize yield, biomass, and ET
394 (Figure 9), but to different degrees. The highest modeled improvement was identified
395 in CLM-crop, with an increase of 57%, 43% and 32% in yield, biomass and ET ,
396 respectively. However, all models except CLM-crop failed to reproduce the growing
397 stage extension under irrigation (Figure 9), probably because only CLM-crop
398 implemented canopy energy balance module to simulate canopy temperature. CLM-
399 crop was thus the only model able to capture the irrigation-induced evaporative
400 cooling effect (the heat-stress reduction). That the best agreement between observed
401 and modeled results occurred with the only model that plausibly accounted for heat-
402 stress alleviation due to irrigation was further evidence that this was the phenomenon
403 we captured in our satellite observational study.

404 **4. Discussion and conclusion**

405 By integrating satellite products and ground-based information about cropping and
406 irrigation, we showed that irrigated maize yields were higher than rainfed maize



407 yields because added irrigation water reduced heat stress in addition to water stress.
408 Our study underlines the relative importance of heat stress alleviation in yield
409 improvement and the necessity of incorporating crop canopy temperature models to
410 better characterize heat stress impacts on crop yields (Teixeira et al., 2013; Kar and
411 Kumar, 2007). Our analysis disentangling the relative importance of heat and water
412 stress alleviation in yield benefit helps farmers plan future investments, especially in
413 terms of selecting cultivars with heat or drought stress tolerance. In addition,
414 disentangling the two effects allows crop models better predict crop phenology,
415 considering irrigation induced cooling effect alters maize growing phases.

416

417 Although ours is not the first study to suggest replace air temperature with MODIS
418 LST for maize yield prediction, especially under extreme warm and dry conditions,
419 our results underscore important implications of doing so. Given the important role of
420 heat stress in determining crop yield, thermal band derived LST information at finer
421 spatial and temporal resolution should be a critical input for satellite data driven yield
422 prediction models (Wang et al., 2015; Huryňa et al., 2019; Li et al., 2019; Meerdink et
423 al., 2019). In addition, given the differential responses of crop growth to heat and
424 water stresses in different stages, fusing satellite derived crop stage information with
425 the heat and water stressors might improve crop yield prediction.

426

427 This study also has useful implications for process-based crop model development. In
428 our model evaluation procedure, only one model has implemented canopy energy
429 balance scheme, but it is the one that captures the observed maize growth stage
430 extension. Our results suggest that the heat stress alleviation due to irrigation
431 identified here is largely overlooked in current crop models. As such, when those crop
432 models are calibrated to match observed yields, processes associated with water stress
433 alleviation are probably overestimated, resulting in uncertainties for predicting future
434 irrigation water demand and crop yield. These uncertainties might mislead future
435 adaptation decisions due to incomplete or biased estimates of the relative
436 contributions of heat and water stress. Relatedly, recent studies identified a wide
437 range for the simulated canopy temperature in current crop models (Webber et al.,
438 2017). Therefore, assimilating satellite derived LST might be a potential solution to
439 improving heat stress representation (Meng et al., 2009; Xu et al., 2011), especially
440 given that the recent ECOSystem Spaceborne Thermal Radiometer Experiment on



441 Space Station (ECOSTRESS) mission makes hourly plant temperature measurement
442 available (Meerdink et al., 2019).

443

444 Several limitations and caveats apply to our study. First, the daily MODIS daytime
445 LST we used to explain crop maximum daily temperature had missing value due to
446 quality control and was derived from a mix of crop covers and other land surface
447 temperature information, which might bias the identified irrigation cooling effect.
448 Specifically, using MODIS daytime LST as a proxy for true (measured) maximum
449 crop surface temperature in an empirical statistical model might underestimate the
450 benefit of cooling effect (measurement error in a predictor variable producing
451 attenuation bias). These uncertainties in LST dataset might be resolved with the
452 recently launched ECOSTRESS mission, as its hourly revisiting frequency enables
453 better estimation of maximum daily temperature. The second issue is that water stress
454 and heat stress were not perfectly separable. As what we have shown, the cooling
455 effect of irrigation lowers evaporative demand (PET) and thus indirectly contributes
456 to lower water stress (higher ET/PET). Our disentangling method do not account for
457 the water stress and heat stress interaction effects. If these interaction effects were
458 considered, the relative contribution of heat stress alleviation to yield improvement is
459 likely to be higher. Such water and heat stress interactions can become stronger
460 during extreme years, like 2012, when most of the Midwest experienced severe
461 drought. Under such circumstances, irrigation-induced cooling effect will be more
462 beneficial. The third issue is that our study is conducted for maize in only one state,
463 Nebraska. Although Nebraska is the largest irrigation maize producer in the US,
464 results might differ for other crop types and other landscapes, due to different crop
465 canopy structures and management practices (Chen et al., 2018), and spatial variations
466 in water and heat stresses mitigation effects (Figure 3 and Figure 7).

467

468 Overall, our study suggests that heat stress alleviation, in addition to water stress
469 alleviation, plays an important role in improving irrigated maize yield. Since current
470 models generally cannot accurately simulate the canopy temperature, the irrigation
471 induced yield benefit might have been overly attributed to water stress alleviation.
472 This might bias the future yield prediction under irrigation, since high temperature
473 stress might be more dominant than drought for crop yield formation under future
474 warmer climate (Zhu et al, 2019; Jin et al., 2017). Therefore, better constrained crop



475 models through integrating satellite observed land surface temperature and crop stage
476 information will be necessary to improve yield prediction and help policymakers and
477 farmers make better decisions on where and when to implement irrigation.
478



479 **References**

- 480 Autovino, D., Minacapilli, M. and Provenzano, G.: Modelling bulk surface resistance
481 by MODIS data and assessment of MOD16A2 evapotranspiration product in an
482 irrigation district of Southern Italy, *Agric. Water Manag.*, 167, 86–94,
483 doi:10.1016/j.agwat.2016.01.006, 2016.
- 484 Bonfils, C. and Lobell, D.: Empirical evidence for a recent slowdown in irrigation-
485 induced cooling, *Proc. Natl. Acad. Sci. U. S. A.*, 104(34), 13582–13587,
486 doi:10.1073/pnas.0700144104, 2007.
- 487 Bruinsma, J.: The resource outlook to 2050: by how much do land, water and crop
488 yields need to increase by 2050?
489 <ftp://ftp.fao.org/docrep/fao/012/ak971e/ak971e00.pdf>, 2009.
- 490 Chen, F., Xu, X., Barlage, M., Rasmussen, R., Shen, S., Miao, S. and Zhou, G.:
491 Memory of irrigation effects on hydroclimate and its modeling challenge,
492 *Environ. Res. Lett.*, 13(6), doi:10.1088/1748-9326/aab9df, 2018.
- 493 Deines, J. M., Kendall, A. D. and Hyndman, D. W.: Annual Irrigation Dynamics in
494 the U.S. Northern High Plains Derived from Landsat Satellite Data, *Geophys.*
495 *Res. Lett.*, 44(18), 9350–9360, doi:10.1002/2017GL074071, 2017.
- 496 DeLucia, E. H., Chen, S., Guan, K., Peng, B., Li, Y., Gomez-Casanovas, N., Kantola,
497 I. B., Bernacchi, C. J., Huang, Y., Long, S. P. and Ort, D. R.: Are we
498 approaching a water ceiling to maize yields in the United States?, *Ecosphere*,
499 10(6), doi:10.1002/ecs2.2773, 2019.
- 500 Egli, D. B.: Seed- Fill Duration and Yield Of Grain Crops, *Adv. Agron.*, 83(C), 243–
501 279, doi:10.1016/S0065-2113(04)83005-0, 2004.
- 502 Elliott, J., Müller, C., Deryng, D., Chryssanthacopoulos, J., Boote, K. J., Böhnner, M.,
503 Foster, I., Glotter, M., Heinke, J., Iizumi, T., Izaurralde, R. C., Mueller, N. D.,
504 Ray, D. K., Rosenzweig, C., Ruane, A. C. and Sheffield, J.: The Global Gridded
505 Crop Model intercomparison: data and modeling protocols for Phase 1 (v1.0),
506 *Geosci. Model Dev.*, 8, 261–277. <https://doi.org/10.5194/gmd-8-261-2015>
- 507 Felfelani, F., Pokhrel, Y., Guan, K. and Lawrence, D. M.: Utilizing SMAP Soil
508 Moisture Data to Constrain Irrigation in the Community Land Model, *Geophys.*
509 *Res. Lett.*, 45(23), 12,892-12,902, doi:10.1029/2018GL080870, 2018..



- 510 Gitelson, A. A.: Wide Dynamic Range Vegetation Index for Remote Quantification of
511 Biophysical Characteristics of Vegetation, *J. Plant Physiol.*, 161(2), 165–173,
512 doi:10.1078/0176-1617-01176, 2004.
- 513 Howell, T. A.: Enhancing water use efficiency in irrigated agriculture, *Agron J*, vol.
514 93, pp. 281–289., 2001.
- 515 Huryňa, H., Cohen, Y., Karnieli, A., Panov, N., Kustas, W. P. and Agam, N.:
516 Evaluation of TsHARP utility for thermal sharpening of Sentinel-3 satellite
517 images using Sentinel-2 visual imagery, *Remote Sens.*, 11(19),
518 doi:10.3390/rs11192304, 2019.
- 519 Jalilvand, E., Tajrishy, M., Ghazi Zadeh Hashemi, S. A. and Brocca, L.:
520 Quantification of irrigation water using remote sensing of soil moisture in a
521 semi-arid region, *Remote Sens. Environ.*, 231, doi:10.1016/j.rse.2019.111226,
522 2019.
- 523 Jin, Z., Zhuang, Q., Wang, J., Archontoulis, S. V., Zobel, Z. and Kotamarthi, V. R.:
524 The combined and separate impacts of climate extremes on the current and future
525 US rainfed maize and soybean production under elevated CO₂, *Glob. Chang.*
526 *Biol.*, 23(7), 2687 – 2704, doi:10.1111/gcb.13617, 2017.
- 527 Johnson, D. M.: A comprehensive assessment of the correlations between field crop
528 yields and commonly used MODIS products, *Int. J. Appl. Earth Obs. Geoinf.*,
529 52, 65–81, doi:10.1016/j.jag.2016.05.010, 2016.
- 530 Kang, S. and Eltahir, E. A. B.: Impact of Irrigation on Regional Climate Over Eastern
531 China, *Geophys. Res. Lett.*, 46(10), 5499–5505, doi:10.1029/2019GL082396,
532 2019.
- 533 Kar, G. and Kumar, A.: Surface energy fluxes and crop water stress index in
534 groundnut under irrigated ecosystem, *Agric. For. Meteorol.*, 146(1–2), 94–106,
535 doi:10.1016/j.agrformet.2007.05.008, 2007.
- 536 Ke, Y., Im, J., Park, S. and Gong, H.: Downscaling of MODIS One kilometer
537 evapotranspiration using Landsat-8 data and machine learning approaches,
538 *Remote Sens.*, 8(3), doi:10.3390/rs8030215, 2016.
- 539 Lawston, P. M., Santanello, J. A. and Kumar, S. V.: Irrigation Signals Detected From
540 SMAP Soil Moisture Retrievals, *Geophys. Res. Lett.*, 44(23), 11,860–11,867,
541 doi:10.1002/2017GL075733, 2017.



- 542 Li, Y., Guan, K., Yu, A., Peng, B., Zhao, L., Li, B. and Peng, J.: Toward building a
543 transparent statistical model for improving crop yield prediction: Modeling
544 rainfed corn in the U.S, *F. Crop. Res.*, 234, 55–65,
545 doi:10.1016/j.fcr.2019.02.005, 2019.
- 546 Loarie, S. R., Lobell, D. B., Asner, G. P., Mu, Q. and Field, C. B.: Direct impacts on
547 local climate of sugar-cane expansion in Brazil, *Nat. Clim. Chang.*, 1(2), 105–
548 109, doi:10.1038/nclimate1067, 2011.
- 549 Meerdink, S. K., Hook, S. J., Roberts, D. A. and Abbott, E. A.: The ECOSTRESS
550 spectral library version 1.0, *Remote Sens. Environ.*, 230,
551 doi:10.1016/j.rse.2019.05.015, 2019.
- 552 Meng, C. L., Li, Z. L., Zhan, X., Shi, J. C. and Liu, C. Y.: Land surface temperature
553 data assimilation and its impact on evapotranspiration estimates from the
554 common land model, *Water Resour. Res.*, 45(2), doi:10.1029/2008WR006971,
555 2009.
- 556 Messina, C. D., Podlich, D., Dong, Z., Samples, M. and Cooper, M.: Yield-trait
557 performance landscapes: From theory to application in breeding maize for
558 drought tolerance, *J. Exp. Bot.*, 62(3), 855–868, doi:10.1093/jxb/erq329, 2011.
- 559 Mu, Q., Zhao, M. and Running, S. W.: Improvements to a MODIS global terrestrial
560 evapotranspiration algorithm, *Remote Sens. Environ.*, 115(8), 1781–1800,
561 doi:10.1016/j.rse.2011.02.019, 2011.
- 562 Mu, Q., Zhao, M., Kimball, J. S., McDowell, N. G. and Running, S. W.: A remotely
563 sensed global terrestrial drought severity index, *Bull. Am. Meteorol. Soc.*, 94(1),
564 83–98, doi:10.1175/BAMS-D-11-00213.1, 2013.
- 565 Müller, C., Elliott, J., Kelly, D., Arneeth, A., Balkovic, J., Ciais, P., Deryng, D.,
566 Folberth, C., Hoek, S., Izaurrealde, R. C., Jones, C. D., Khabarov, N., Lawrence,
567 P., Liu, W., Olin, S., Pugh, T. A. M., Reddy, A., Rosenzweig, C., Ruane, A. C.,
568 Sakurai, G., Schmid, E., Skalsky, R., Wang, X., de Wit, A. and Yang, H.: The
569 Global Gridded Crop Model Intercomparison phase 1 simulation dataset, *Sci.
570 Data*, 6(1), doi:10.1038/s41597-019-0023-8, 2019.
- 571 Niu, J., Shen, C., Li, S. G. and Phanikumar, M. S.: Quantifying storage changes in
572 regional Great Lakes watersheds using a coupled subsurface-land surface process
573 model and GRACE, MODIS products, *Water Resour. Res.*, 50(9), 7359–7377,
574 doi:10.1002/2014WR015589, 2014.



- 575 Peng, S. S., Piao, S., Zeng, Z., Ciais, P., Zhou, L., Li, L. Z. X., Myneni, R. B., Yin, Y.
576 and Zeng, H.: Afforestation in China cools local land surface temperature, Proc.
577 Natl. Acad. Sci. U. S. A., 111(8), 2915–2919, doi:10.1073/pnas.1315126111,
578 2014.
- 579 Rosegrant, M.W., Cai, X. and Cline, S.: World Water and Food to 2025: Dealing
580 with Scarcity, Food Policy. <https://doi.org/10.1098/rstb.2005.1744>, 2002.
- 581 Ruiz-Vera, U.M., Siebers, M.H., Jaiswal, D., Ort, D.R. and Bernacchi, C.J.: Canopy
582 warming accelerates development in soybean and maize, offsetting the delay in
583 soybean reproductive development by elevated CO₂ concentrations. Plant Cell
584 Environ. 41, 2806–2820. <https://doi.org/10.1111/pce.13410>, 2018.
- 585 Running, S.W., Mu, Q., Zhao, M. and Moreno, A.: Modis Global Terrestrial
586 Evapotranspiration (ET) Product (NASA MOD16A2/A3) NASA Earth
587 Observing System Modis Land Algorithm. NASA: Washington, DC, USA.
- 588 Russo, S., Dosio, A., Graversen, R. G., Sillmann, J., Carrao, H., Dunbar, M. B.,
589 Singleton, A., Montagna, P., Barbola, P. and Vogt, J. V.: Magnitude of extreme
590 heat waves in present climate and their projection in a warming world, J.
591 Geophys. Res. Atmos., 119(22), 12,500–12,512, doi:10.1002/2014JD022098,
592 2014.
- 593 Sacks, W. J., Cook, B. I., Buening, N., Levis, S. and Helkowski, J. H.: Effects of
594 global irrigation on the near-surface climate, Clim. Dyn., 33(2–3), 159–175,
595 doi:10.1007/s00382-008-0445-z, 2009.
- 596 Siebert, S. and Döll, P.: Quantifying blue and green virtual water contents in global
597 crop production as well as potential production losses without irrigation, J.
598 Hydrol., 384(3–4), 198–217, doi:10.1016/j.jhydrol.2009.07.031, 2010.
- 599 Siebert, S., Webber, H., Zhao, G. and Ewert, F.: Heat stress is overestimated in
600 climate impact studies for irrigated agriculture, Environ. Res. Lett., 12(5),
601 doi:10.1088/1748-9326/aa702f, 2017.
- 602 Siebert, S., Ewert, F., Eyshi Rezaei, E., Kage, H. and Graß, R.: Impact of heat stress
603 on crop yield - On the importance of considering canopy temperature, Environ.
604 Res. Lett., 9(4), doi:10.1088/1748-9326/9/4/044012, 2014.
- 605 Tack, J., Barkley, A. and Hendricks, N.: Irrigation offsets wheat yield reductions from
606 warming temperatures, Environ. Res. Lett., 12(11), doi:10.1088/1748-
607 9326/aa8d27, 2017.



- 608 Teixeira, E. I., Fischer, G., Van Velthuizen, H., Walter, C. and Ewert, F.: Global hot-
609 spots of heat stress on agricultural crops due to climate change, *Agric. For.*
610 *Meteorol.*, 170, 206–215, doi:10.1016/j.agrformet.2011.09.002, 2013.
- 611 Teuling, A. J., Seneviratne, S. I., Stöckli, R., Reichstein, M., Moors, E., Ciais, P.,
612 Luysaert, S., Van Den Hurk, B., Ammann, C., Bernhofer, C., Dellwik, E.,
613 Gianelle, D., Gielen, B., Grünwald, T., Klumpp, K., Montagnani, L., Moureaux,
614 C., Sottocornola, M. and Wohlfahrt, G.: Contrasting response of European forest
615 and grassland energy exchange to heatwaves, *Nat. Geosci.*, 3(10), 722–727,
616 doi:10.1038/ngeo950, 2010.
- 617 Thiery, W., Davin, E. L., Lawrence, D. M., Hirsch, A. L., Hauser, M. and
618 Seneviratne, S. I.: Present-day irrigation mitigates heat extremes, *J. Geophys.*
619 *Res.*, 122(3), 1403–1422, doi:10.1002/2016JD025740, 2017.
- 620 Thornton, P. E., Thornton, M. M., Mayer, B. W., Wei, Y., Devarakonda, R., Vose, R.
621 S. and Cook, R. B.: Daymet: Daily Surface Weather Data on a 1-km Grid for
622 North America, Version 3, Version 3. ORNL DAAC, Oak Ridge, Tennessee,
623 USA [online] Available from: <https://search.earthdata.nasa.gov/search>, 2018.
- 624 Tomlinson, C. J., Chapman, L., Thornes, J. E. and Baker, C. J.: Derivation of
625 Birmingham’s summer surface urban heat island from MODIS satellite images,
626 *Int. J. Climatol.*, 32(2), 214–224, doi:10.1002/joc.2261, 2012.
- 627 Troy, T. J., Kipgen, C. and Pal, I.: The impact of climate extremes and irrigation on
628 US crop yields, *Environ. Res. Lett.*, 10(5), doi:10.1088/1748-9326/10/5/054013,
629 2015
- 630 US Department of Agriculture (USDA) NASS: Quick Stats: Agricultural Statistics
631 Data Base, Natl. Agric. Stat. Serv., Available from:
632 <http://www.nass.usda.gov/QuickStats/>, 2018a.
- 633 US Department of Agriculture (USDA): Crop Scape and Cropland Data Layer –
634 National Download.
635 https://www.nass.usda.gov/Research_and_Science/Cropland/Release/index.php.
636 2018b
- 637 Wallace, J. S.: Increasing agricultural water use efficiency to meet future food
638 production, *Agric. Ecosyst. Environ.*, 82(1–3), 105–119, doi:10.1016/S0167-
639 8809(00)00220-6, 2000.



- 640 Wan, Z.: New refinements and validation of the MODIS Land-Surface
641 Temperature/Emissivity products, *Remote Sens. Environ.*, 112(1), 59–74,
642 doi:10.1016/j.rse.2006.06.026, 2008.
- 643 Wang, E. and Engel, T.: Simulation of phenological development of wheat crops,
644 *Agric. Syst.*, 58(1), 1–24, doi:10.1016/S0308-521X(98)00028-6, 1998.
- 645 Wang, F., Qin, Z., Song, C., Tu, L., Karnieli, A. and Zhao, S.: An improved mono-
646 window algorithm for land surface temperature retrieval from landsat 8 thermal
647 infrared sensor data, *Remote Sens.*, 7(4), 4268–4289, doi:10.3390/rs70404268,
648 2015.
- 649 Webber, H., Martre, P., Asseng, S., Kimball, B., White, J., Ottman, M., Wall, G. W.,
650 De Sanctis, G., Doltra, J., Grant, R., Kassie, B., Maiorano, A., Olesen, J. E.,
651 Ripoche, D., Rezaei, E. E., Semenov, M. A., Stratonovitch, P. and Ewert, F.:
652 Canopy temperature for simulation of heat stress in irrigated wheat in a semi-arid
653 environment: A multi-model comparison, *F. Crop. Res.*, 202, 21–35,
654 doi:10.1016/j.fcr.2015.10.009, 2017.
- 655 Xu, T., Liu, S., Liang, S. and Qin, J.: Improving predictions of water and heat fluxes
656 by assimilating MODIS land surface temperature products into the Common
657 Land Model, *J. Hydrometeorol.*, 12(2), 227–244, doi:10.1175/2010JHM1300.1,
658 2011.
- 659 Zaussinger, F., Dorigo, W., Gruber, A., Tarpanelli, A., Filippucci, P. and Brocca, L.:
660 Estimating irrigation water use over the contiguous United States by combining
661 satellite and reanalysis soil moisture data, *Hydrol. Earth Syst. Sci.*, 23(2), 897–
662 923, doi:10.5194/hess-23-897-2019, 2019.
- 663 Zhu, P., Jin, Z., Zhuang, Q., Ciais, P., Bernacchi, C., Wang, X., Makowski, D. and
664 Lobell, D.: The important but weakening maize yield benefit of grain filling
665 prolongation in the US Midwest, *Glob. Chang. Biol.*, 24(10), 4718–4730,
666 doi:10.1111/gcb.14356, 2018.
- 667 Zhu, P., Zhuang, Q., Archontoulis, S. V., Bernacchi, C. and Müller, C.: Dissecting the
668 nonlinear response of maize yield to high temperature stress with model-data
669 integration, *Glob. Chang. Biol.*, 25(7), 2470–2484, doi:10.1111/gcb.14632,
670 2019.

671

672 **Acknowledgments**

673

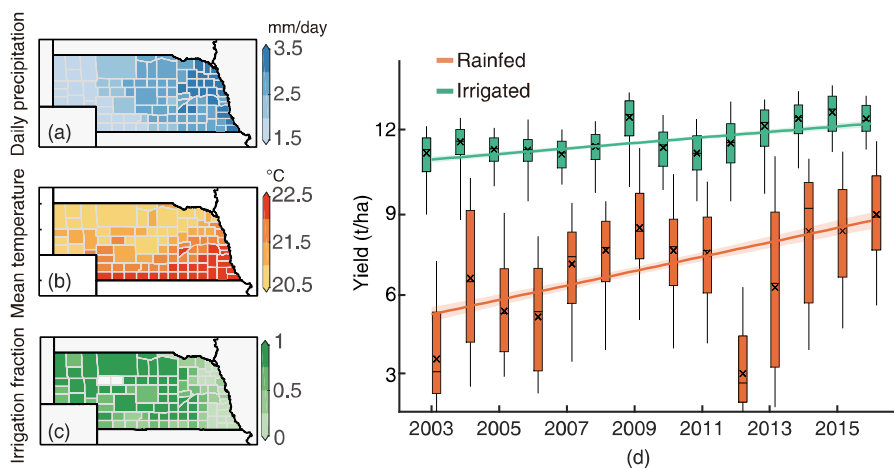


674 We thank the NSF/USDA NIFA INFEWS T1 #1639318 for funding support.

675



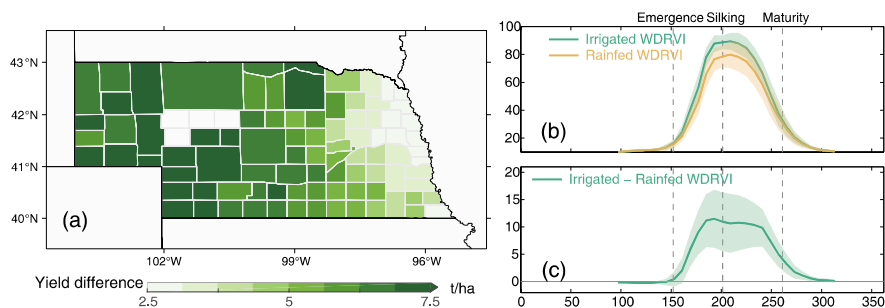
676 **Figures**



677

678 **Figure 1:** The spatial pattern of county level multi-year (2003-2016) mean daily
 679 precipitation (a) and air temperature (b) during maize growing season. County level
 680 multi-year (2003-2016) mean maize irrigation fraction across Nebraska (c). The
 681 maize irrigation fraction is based on USDA NASS report. Boxplot of county level
 682 irrigated and rainfed maize yield in Nebraska over the study period (d). The lines in (d)
 683 show the linear fitted yield trend with 95% confidence interval. Boxplots indicate the
 684 median (horizontal line), mean (cross), inter-quartile range (box), and 5–95th
 685 percentile (whiskers) of rainfed or irrigated yield across all counties.

686

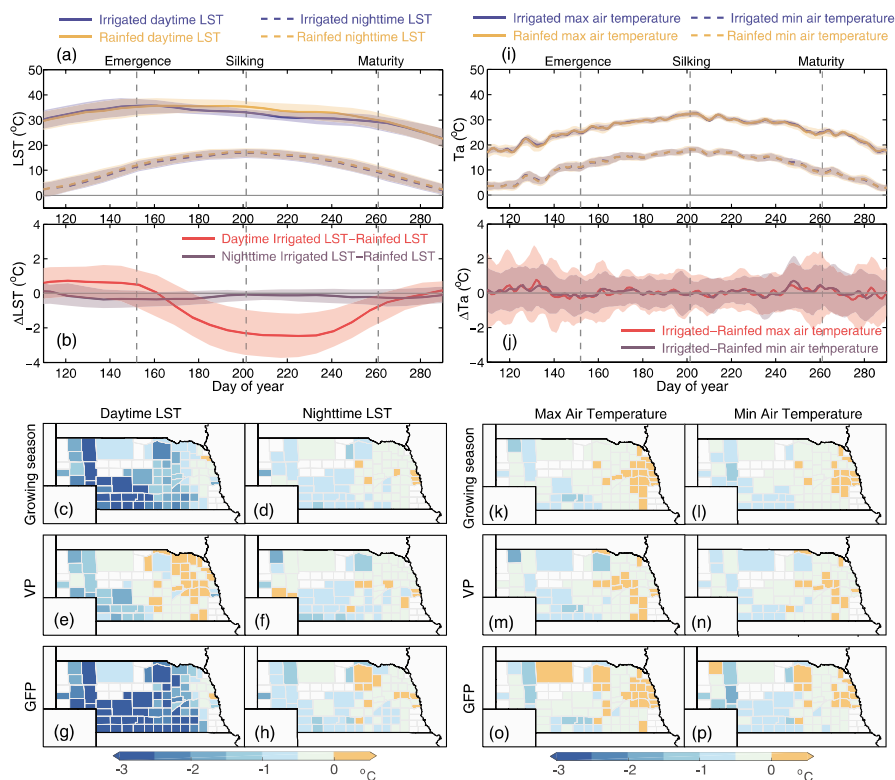


687

688 **Figure 2:** The difference between irrigated and rainfed maize yield (a) and satellite
 689 observed vegetation index (b and c). The shaded area in (b) and (c) shows one
 690 standard deviation of WDRVI (b) and WDRVI difference (c).

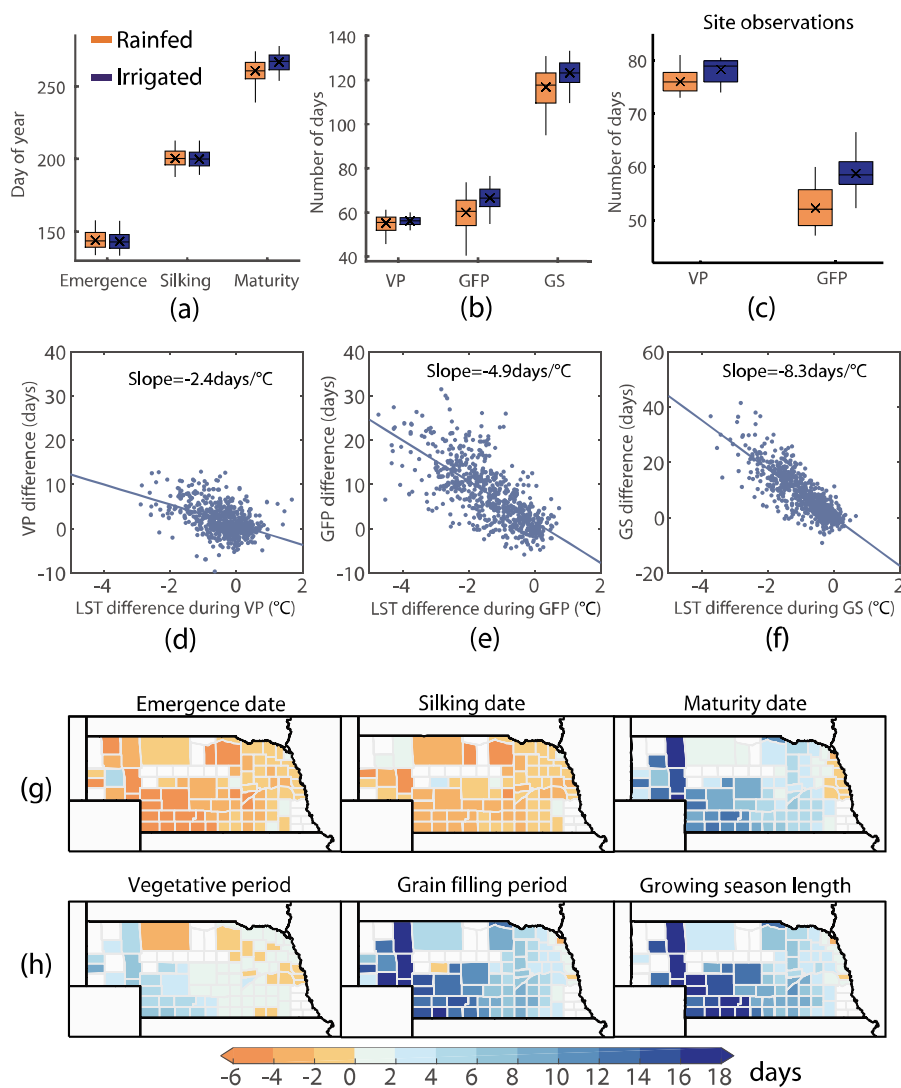
691

692



693
 694 **Figure 3:** Spatial-temporal patterns of daytime and nighttime MODIS LST
 695 differences (left panel, a-h) and surface air temperature differences (right panel, i-p)
 696 between irrigated and rainfed maize in different growth stages: vegetative period and
 697 grain filling period. The shaded areas in (a), (b) and (i), (j) show one standard
 698 deviation of corresponding variables.

699
 700

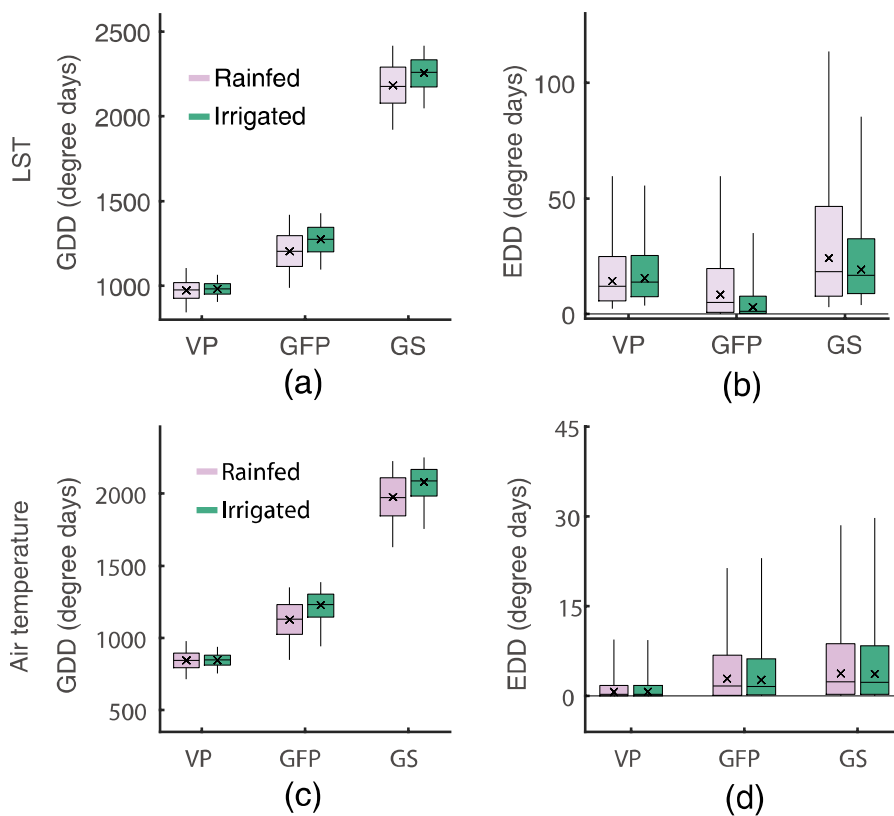


701

702 **Figure 4:** Boxplot of maize phenological date (a) and duration (b-c) for irrigated and
 703 rainfed maize areas. Sensitivity of phenological duration difference between irrigated
 704 and rainfed maize to LST difference between irrigated and rainfed maize (d-f). The
 705 slope in (d-f) was estimated with linear model. The spatial pattern of phenological
 706 date and duration differences between irrigated and rainfed maize areas (g-h).

707

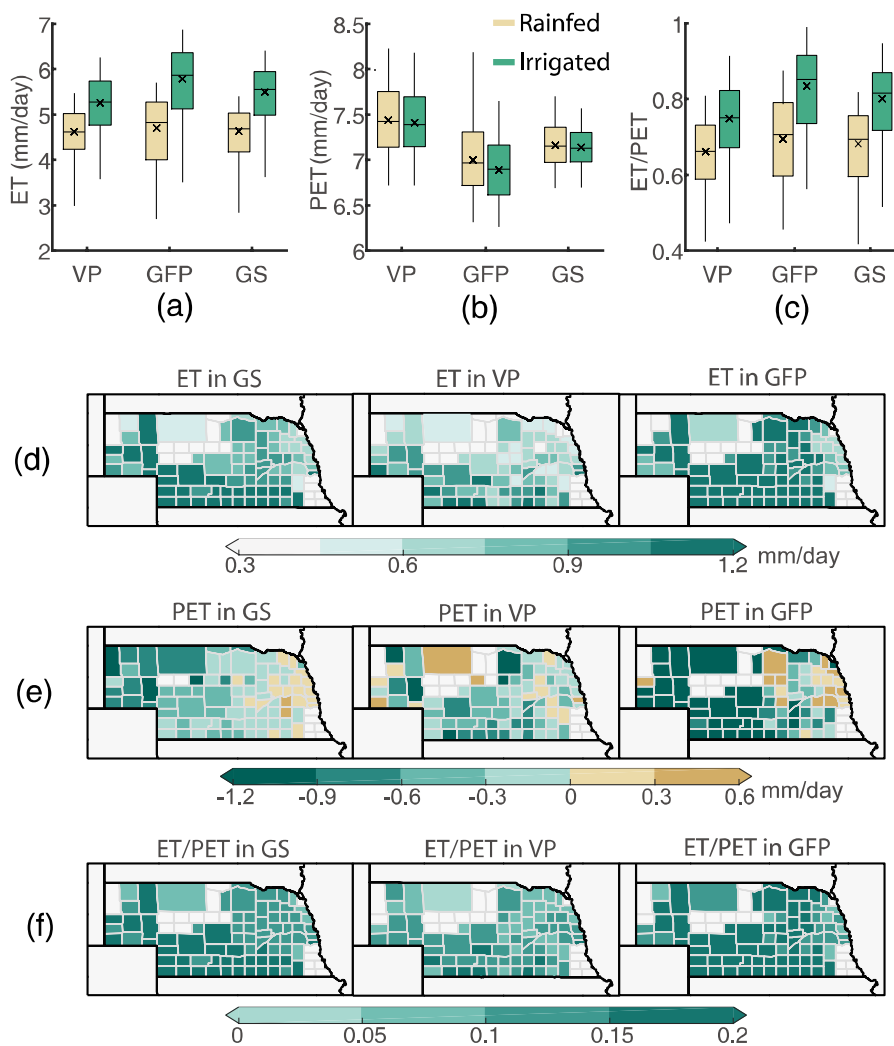
708



709

710 **Figure 5:** Boxplot of GDD and EDD estimated with MODIS LST (a-b) and surface
711 air temperature (c-d) for irrigated and rainfed maize areas. Boxplots indicate the mean
712 (cross), median (horizontal line), 25--75th percentile (box), and 5--95th percentile
713 (whiskers) of corresponding variables in all year and county combinations.

714

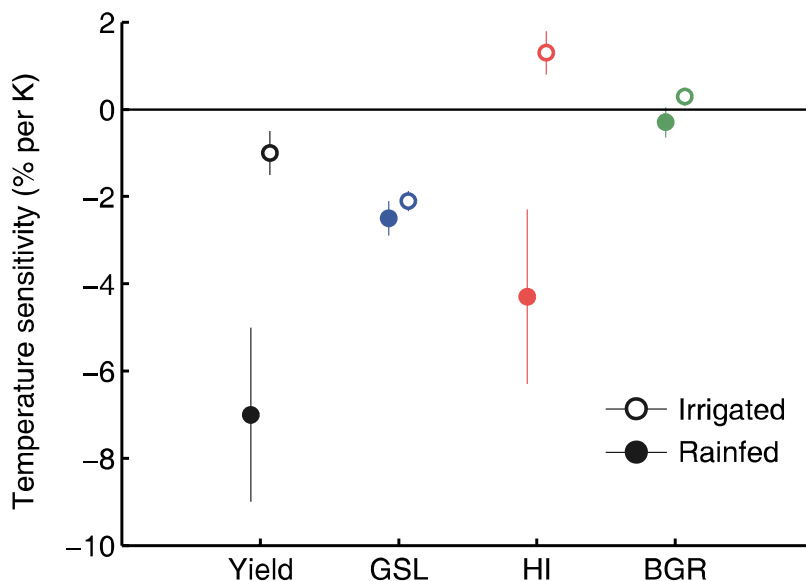


715

716

717 **Figure 6:** Boxplot of SSEBop ET, MODIS PET and ET/PET for irrigated and rainfed
718 maize areas (a-c). Spatial pattern of SSEBop ET, MODIS PET and ET/PET
719 differences between irrigated and rainfed maize areas (d-f).

720



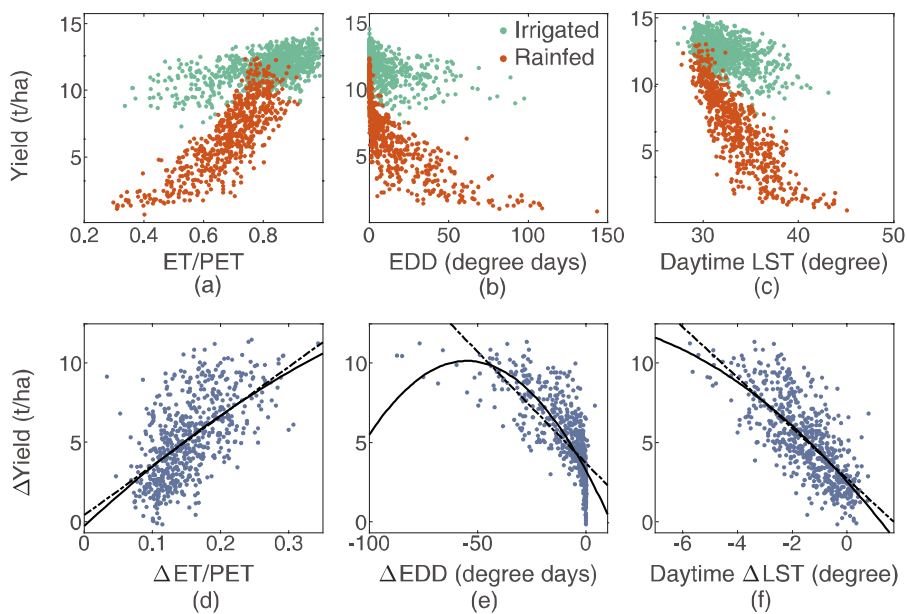
721

722 **Figure 7:** Temperature sensitivity of yield and yield components (GSL, HI and BGR)

723 for irrigated and rainfed maize areas.

724

725



726

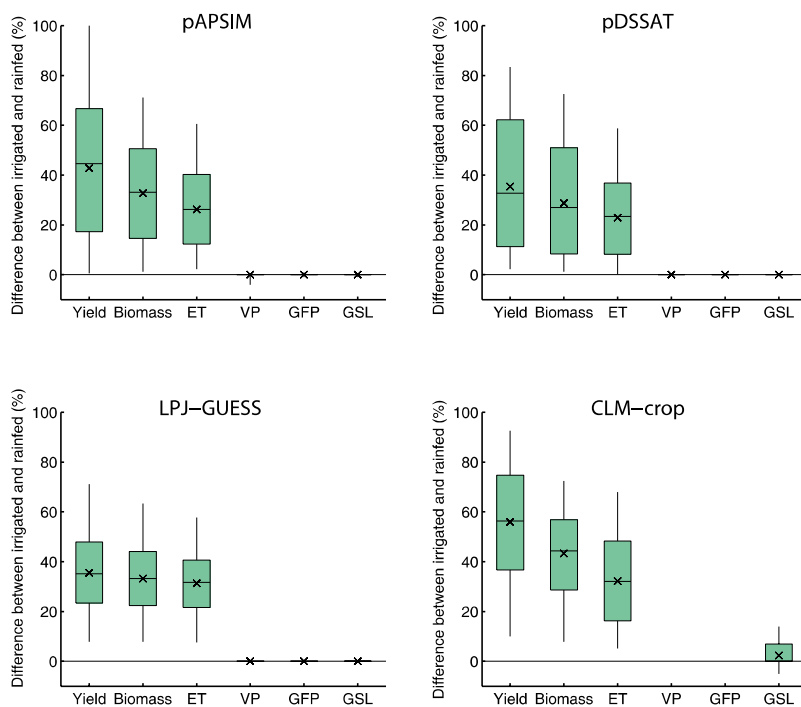


727 **Figure 8:** Response of maize yield to ET/PET (a), EDD (b) and daytime LST (c) in
728 both irrigated and rainfed maize. Response of yield differences to ET/PET (d), EDD
729 (e) and daytime LST (f) differences between irrigated and rainfed maize. The linear
730 (dash black line) and quadratic (solid black line) response curves of $\Delta Yield$ to
731 $\Delta ET/PET$, ΔEDD and ΔLST are shown in d-f.

732

733

734



735

736 **Figure 9:** Boxplot of crop model simulated yield, biomass, ET and phenological
737 duration (VP, GFP and GSL) differences between irrigated and rainfed maize.
738 For phenological duration, CLM-crop only reports GSL.

Supplemental figures

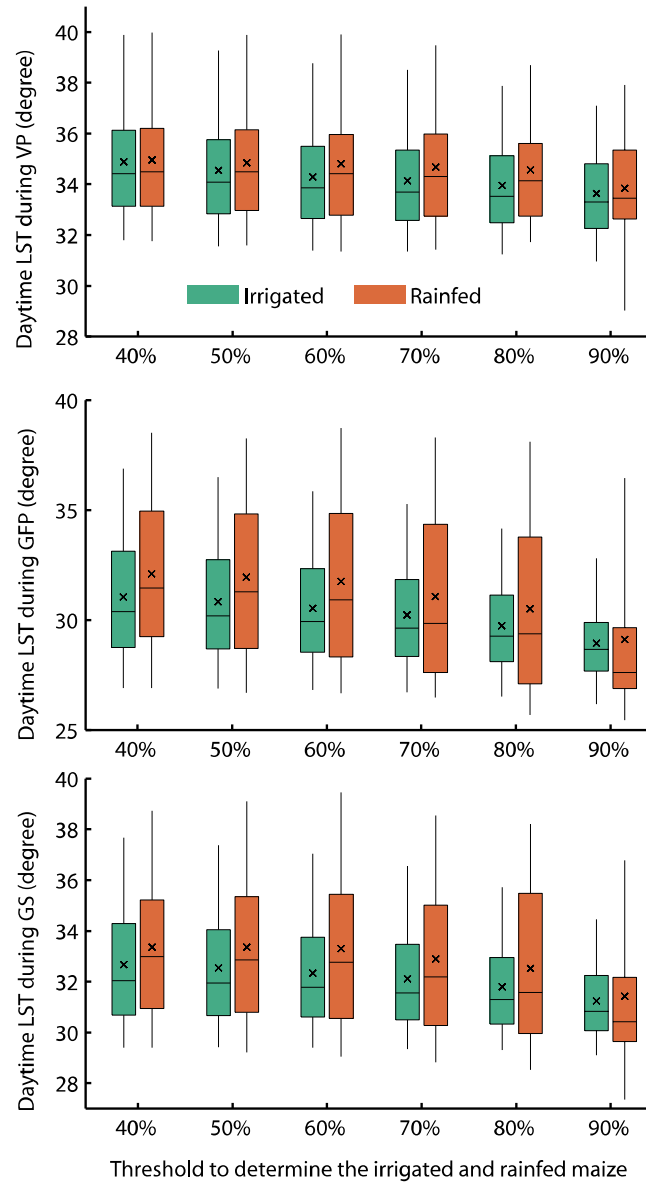


Figure S1 Boxplot of LST during VP, GFP and growing season with different thresholds to determine the irrigated and rainfed maize cropland. Boxplots indicate the mean (cross line), median (horizontal line), 25--75th percentile (box), and 5--95th percentile (whiskers) of county level LST for all year and county combinations.

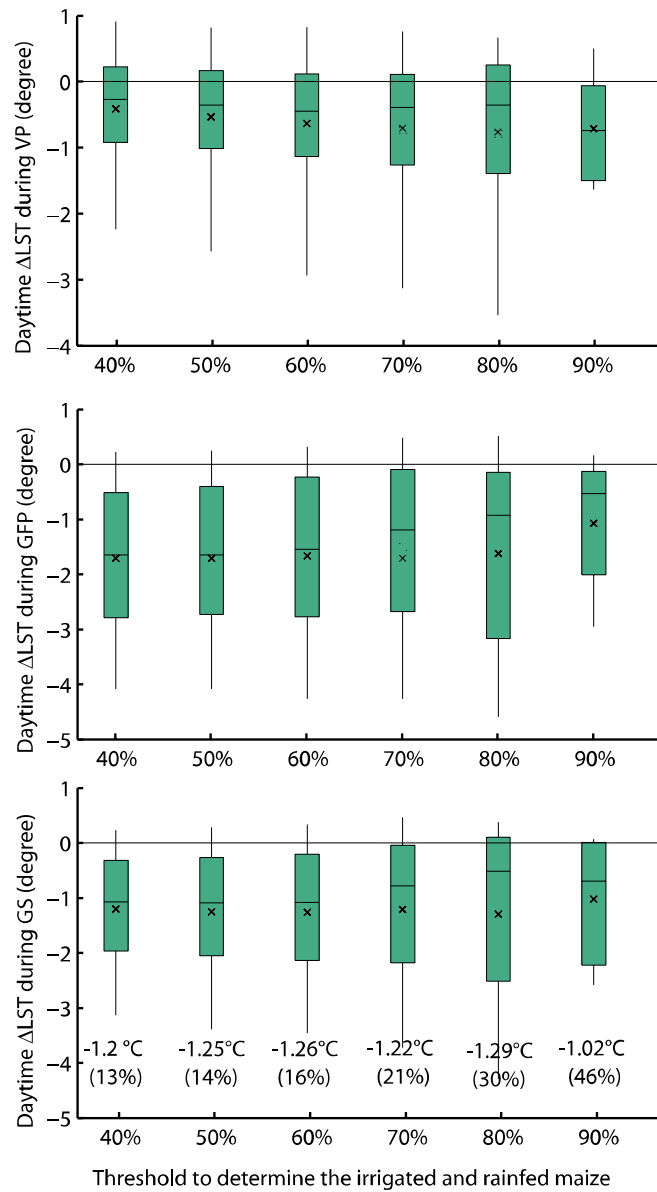


Figure S2 Boxplot of LST difference between irrigated and rainfed maize during VP, GFP and growing season with different thresholds to determine the irrigated and rainfed maize cropland. Boxplots indicate the mean (cross line), median (horizontal line), 25--75th percentile (box), and 5--95th percentile (whiskers) of county level LST difference for all year and county combinations. The numbers below the boxplot indicated the mean LST difference during GS. The numbers within parentheses indicated the percentage of counties omitted in the boxplot statistics since some counties did not have pixels satisfying the high threshold.

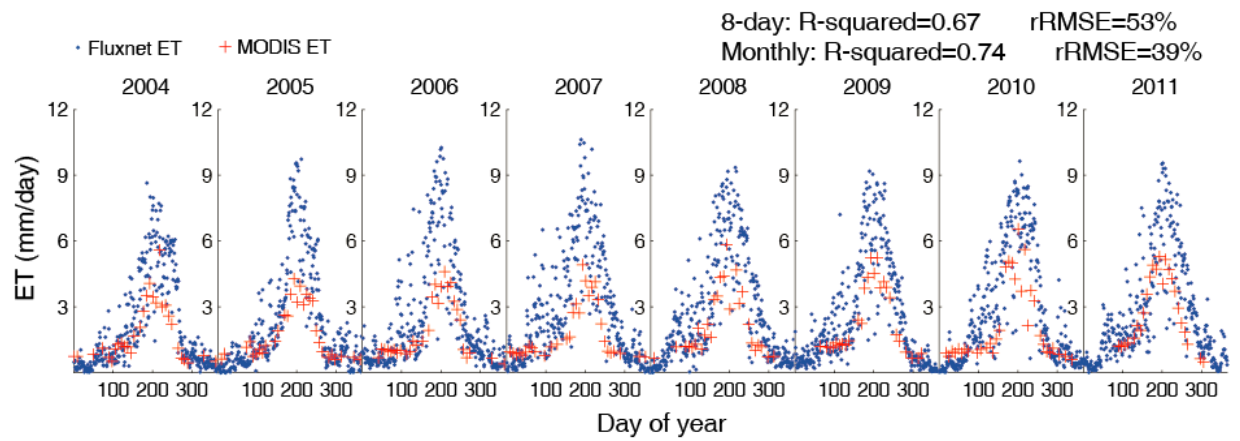


Figure S3 Comparison of MODIS ET and Fluxnet observed daily ET during 2004-2011.

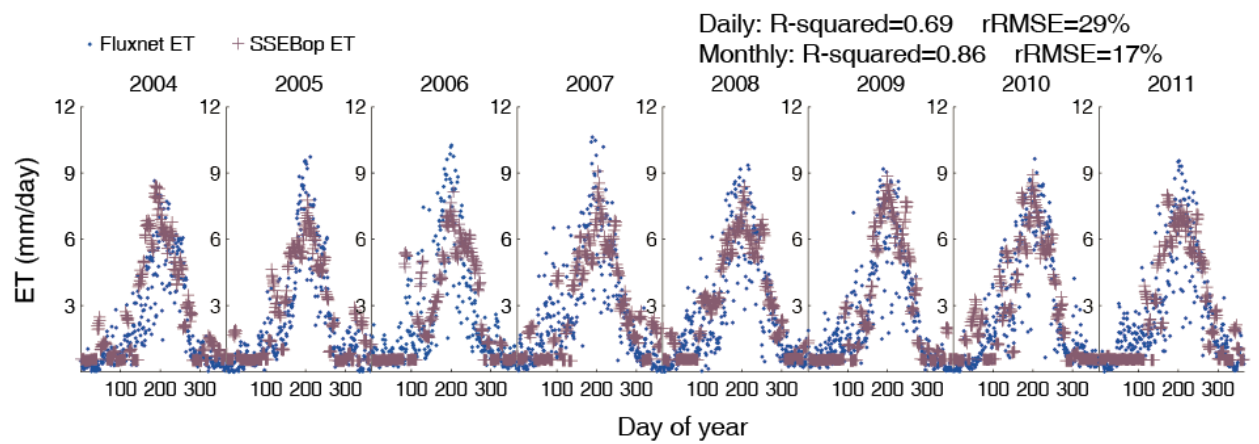


Figure S4 Comparison of SSEBop ET and Fluxnet observed daily ET during 2004-2011.

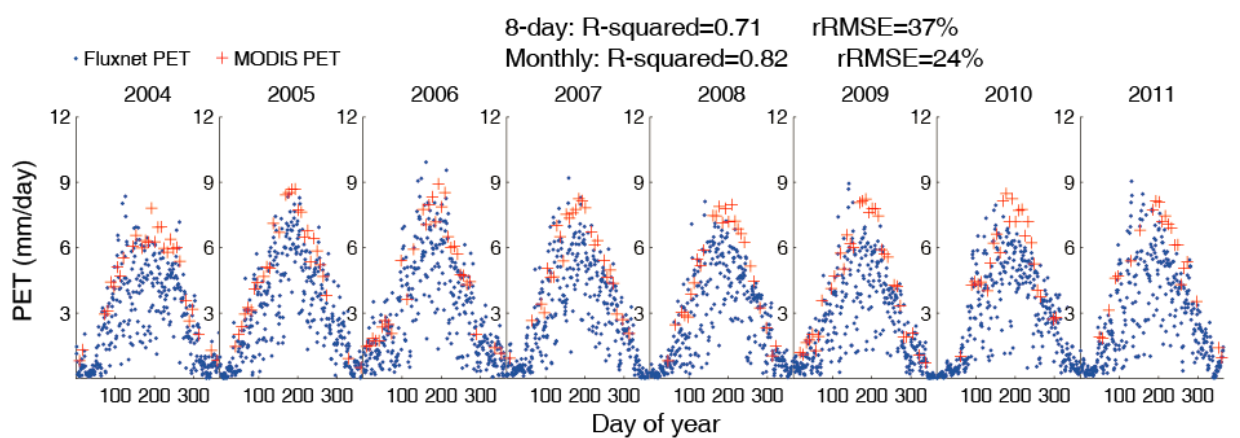


Figure S5 Comparison of MODIS PET and Fluxnet estimated daily PET during 2004-2011. Fluxnet PET is estimated with Penman–Monteith equation with site measured meteorological variables as the forcing data.